Flow Field Simulations of a Gas Turbine Combustor

M. D. Barringer
O. T. Richard
J. P. Walter
S. M. Stitzel
K. A. Thole

Mechanical Engineering Department,
Virginia Polytechnic Institute and
State University,
Blacksburg, VA 24061

The flow field exiting the combustor in a gas turbine engine is quite complex considering the presence of large dilution jets and complicated cooling schemes for the combustor liner. For the most part, however, there has been a disconnect between the combustor and turbine when simulating the flow field that enters the nozzle guide vanes. To determine the effects of a representative combustor flow field on the nozzle guide vane, a large-scale wind tunnel section has been developed to simulate the flow conditions of a prototypical combustor. This paper presents experimental results of a combustor simulation with no downstream turbine section as a baseline for comparison to the case with a turbine vane. Results indicate that the dilution jets generate turbulence levels of 15–18% at the exit of the combustor with a length scale that closely matches that of the dilution hole diameter. The total pressure exiting the combustor in the near-wall region neither resembles a turbulent boundary layer nor is it completely uniform putting both of these commonly made assumptions into question. [DOI: 10.1115/1.1475742]

Introduction

A major factor in decreasing the cost of gas turbine engines, whether they be for military or for commercial uses, is to reduce the maintenance costs. The turbine, particularly the first stage, is subject to very harsh conditions resulting from high-temperature and high-turbulence flows exiting the combustor. Operational experience indicates that some turbine airfoils suffer serious damage while adjacent airfoils remain in good operating condition. This observation suggests that there are significant nonuniformities in the exit combustor flows that have detrimental effects on the airfoils.

To evaluate the effects of these nonuniformities and to further our understanding in how to best integrate the combustor and turbine, a new experimental facility was developed to simulate prototypical combustor exit conditions as the entrance conditions to a first stage, linear, turbine vane cascade. Although this study has not simulated the reacting flow, thereby not including such affects as the heat release due to combustion, it is important to recognize that we should begin by determining whether we can computationally simulate the nonreacting flow field. The heat release, for example, will depend upon the mixing characteristics of the dilution jets. If the dilution jets can not be accurately simulated under the nonreacting conditions, it would be difficult to simulate the reacting flow field. For the design of the facility reported in this paper, nonuniformities in both the span (radial) and pitch (circumferential) directions exiting the combustor have been simulated through the use of combustor liner panels, insuring representative near-platform flows, and dilution jets, insuring representative mainstream flows with high levels of turbulence.

In general, the following objectives for the facility described in this paper are: i) to simulate the flow conditions for a prototypical combustor that is nonreacting, ii) to quantify the exit conditions (inlet conditions for the turbine) for this prototypical combustor, and iii) to quantify the flow field in the downstream vane passage as a result of the nonuniform combustor exit conditions. Specifically, this paper presents the effects that the dilution jets have on the flow and thermal fields exiting the combustor with no downstream turbine vane present. This paper describes those experimentally measured flow and thermal fields after describing the development of the combustor simulator facility.

Contributed by the International Gas Turbine Institute and presented at the International Gas Turbine and Aeroengine Congress and Exhibition, New Orleans, Louisiana, June 4–7, 2001. Manuscript received by the IGTI, November 2000; revised manuscript received March 2001. Paper No. 2001-GT-170. Review Chair: R. A. Natole.

Relevant Past Studies

A majority of the past experimental and computational simulations of a gas turbine have assumed either a simple two-dimensional turbulent boundary layer and a uniform mean field or a constant total pressure entering the first stage turbine vane. As a result of a simple two-dimensional turbulent boundary layer assumption, the resulting secondary flow pattern in the vane passage comprises a horseshoe vortex, which splits into two legs; a suction side leg and a pressure side leg that further develops into the passage vortex. This secondary flow pattern was first suggested by Langston [1] and more recently confirmed by measurements of Kang and Thole [2]. As a result of a constant total pressure assumption, no changes in the streamline pattern would occur as theoretically shown by Munk and Prim [3] and computationally shown to be true by Shang and Epstein [4] and Hermanson and Thole [5]. A uniform total pressure field results in no radial pressure gradient, which is needed to drive the passage vortex. Both assumptions, a two-dimensional turbulent boundary layer or a constant total pressure, are questionable for the nozzle guide vane particularly in the hub and tip regions. These are questionable if one considers that as much as 50% or more of the flow entering the main gas path is fluid that has passed through combustor liners in the form of either film coolant or dilution fluid.

While the experimental studies by Butler et al. [6] and Shang et al. [7] have considered nonuniform inlet temperature profiles, the only study to have measured a realistic total pressure variation was that by Stabe et al. [8]. Stabe et al. [8] simulated a liner flow through the use of a combustor exit radial temperature simulator (CERTS). The CERTS used circumferential slots with no dilution holes. This study clearly indicated changes did occur in the total pressure when using the CERTS as compared to not using the CERTS. Details are not available, however, for comparing the effects that the two different total pressure profiles had on the secondary flow field development in the stator vane section.

Burd and Simon [9] simulated a range of injection flows from a two-dimensional slot upstream of a nozzle guide vane. Although this is an important study, the geometry used does not have all of the elements necessary to represent that of a combustor liner for an aeroengine. In their work, they reported to have made a single-point total pressure measurement at the inlet to their vane cascade. They indicated in their paper that the inlet total pressure field was considered to be uniform for the full range of injection to mainstream mass flow ratios. The thermal field results reported by Burd et al. [10], however, indicated that for a mass flow ratio greater than 3.2%, the injectant (coolant) migrated up the pressure

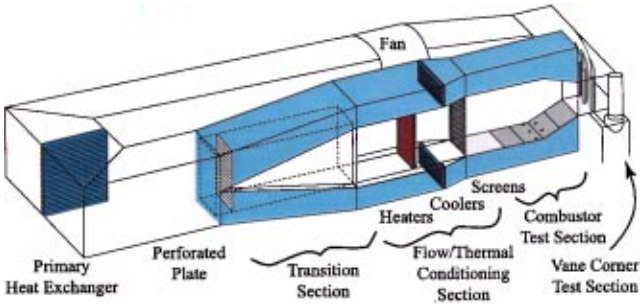

Fig. 1 Illustration of the low speed wind tunnel facility with the combustor simulator section

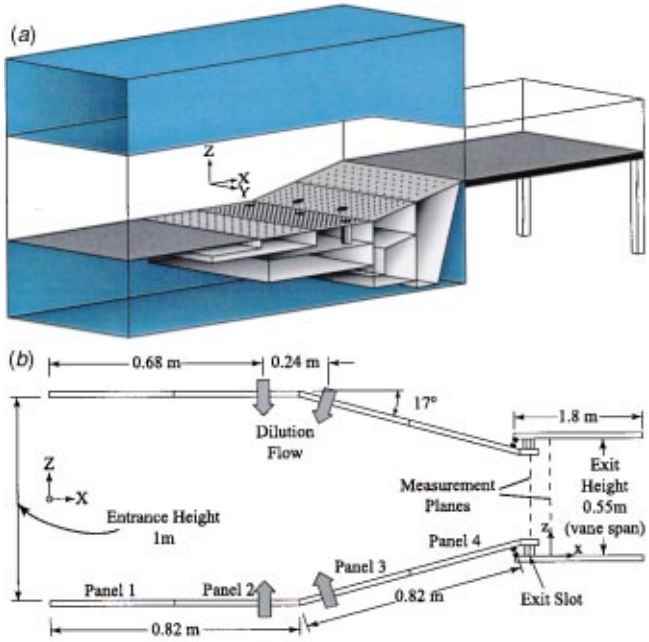

Fig. 2 Illustration of the supply channels for each of the combustor liner and dilution flows (*a*), and geometric details of the primary flow path (*b*).

surface of the vane. This is consistent with having a higher total pressure in the near-wall region. A higher total pressure in the near platform region results in a vortex of opposite rotation as the passage vortex first illustrated by Langston [1]. The results of Burd et al. [10] indicated a vortex that would drive flow up the pressure side of the vane away from the endwall, whereas Langston's passage vortex has the orientation to drive flow down the pressure side of the vane toward the endwall. Recall Langston [1] considered a two-dimensional turbulent boundary layer where the total pressure decreases due to a decrease in velocity as one moves from the midspan to the endwall region. This reversal of the passage vortex was shown to occur computationally by Hermanson and Thole [5] when a higher total pressure occurs in the endwall region.

This summary of relevant literature demonstrates the importance of knowing what the inlet flow conditions are to the first stage vane in the turbine. What is lacking, however, are the needed measurements of the total pressure field and turbulence levels that can be used as boundary conditions for turbine vane simulations. The next logical step in accurately assessing the capabilities of computing turbine flow fields and heat transfer is to evaluate whether the computational codes can accurately simulate these nonuniform inlet flows to the turbine.

Description of Experimental Simulations

Complete measurements of the near wall flows exiting an actual combustor are nearly impossible to achieve in an operating engine. For this purpose, a scaled-up combustor simulator facility was carefully designed to simulate the geometry and flow conditions of an early design of a prototypical aeroengine combustor with these values being provided by industry (Soechting and Cheung [11]). The purpose of making this facility large scale was to allow for good spatial measurement resolution. In general, the wind tunnel simulation included combustor liner panels with many rows of discrete, axially oriented film-cooling holes and two streamwise rows of large dilution holes. At the end of the liner panels, there is a slot in which more coolant is injected into the primary passage. More discussion will follow in this section on the details of the liner panels and exit slot.

The wind tunnel facility itself has been described in numerous previous studies (Kang et al. [12], Kang and Thole [2], and Radomsky and Thole [13,14]) as a closed-loop tunnel with a scaled-up (9X), two passage (one sector), linear cascade. The flow is driven for both the past reported studies as well as the study described in this paper by a single 50-hp axial fan. Downstream of the fan is a large primary heat exchanger core. Somewhat downstream of the heat exchanger core is the linear cascade, which is placed in a corner of the tunnel.

The modifications made to this facility include replacing a 7.3-m long section, located just upstream of the cascade corner test section as illustrated in Fig. 1. The replacement section includes a transition section that splits the flow into a primary flow passage and two symmetric secondary flow passages located on the top and bottom of the primary flow passage. Within the transition section in the primary flow passage, the flow immediately passes through a perforated plate. The sole purpose of the perforated plate is to provide the necessary pressure drop to control the flow splits between the primary and secondary passages. At a distance 3.5 m downstream of the perforated plate, the flow passes through a thermal and flow conditioning section containing a bank of heaters followed by a series of screens and flow straighteners. The heater section comprises three individually controlled banks of electrically powered, finned bars supplying a maximum total heat addition of 55 kW. This total heat addition is enough to raise the primary passage flow to a temperature 20°C above the secondary flow coolant temperature. A controller unit maintains a set point temperature to within 1°C. Downstream of the flow straighteners, the heated primary flow enters the combustor simulator. In the combustor simulator, secondary coolant flow is injected into the primary flow passage through liner panels and dilution holes. In addition, the flow is accelerated prior to entering the turbine section.

The flow in the secondary passages, also shown in Fig. 1, is first directed through heat exchangers. In addition to heat being rejected from the primary heat exchanger, the heat exchangers in the secondary passages provide additional heat rejection for the coolant flow. The flow in the secondary passages is then directed into a large supply chamber as shown in Fig. 2(*a*). This supply chamber provides the flow necessary for the combustor liner cooling and dilution holes. The exit slot is used for the purpose of providing additional cooling to the platform. In the combustor simulator there are a series of four streamwise panels on both the top and the bottom that contain the film-cooling and dilution holes. To insure the correct coolant flow splits among the liner panels and dilution rows, separate supply chambers for each component were placed within the large supply. These separate chambers are also indicated in Fig. 2(*a*). The coolant flow for the exit slot at the end of the combustor panels was maintained by providing the required pressure in the large supply chamber. Fig. 2(*b*) gives the overall dimensions of the combustor simulator.

Velocity and temperature field measurements were made at the inlet to the combustor section using a hot-wire and thermocouple to verify the flow uniformity. The maximum deviation in the mean

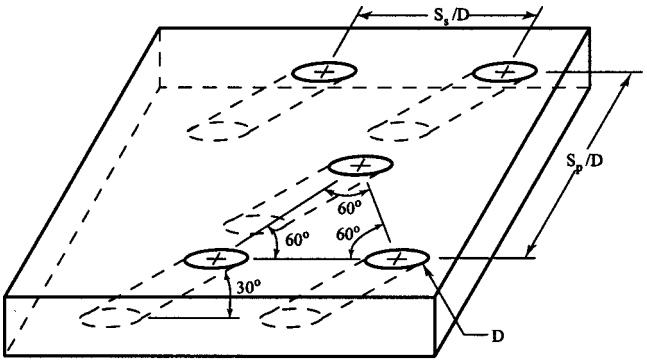

Liner Geometry Feature	S_p/D	S_s/D
Panel 1	10.1	5.8
Panel 2	6.1	3.5
Panel 3	6.1	3.5
Panel 4	10.1	5.8
Dilution Row 1	60 (5.4 D_1)	90.2 (8.1 D_1)
Dilution Row 2	60 (3.8 D_2)	120.8 (7.6 D_2)

Fig. 3 Film-cooling hole pattern for each liner panel

velocity was 1.9%, while the maximum deviation in the temperature was 5.7% (based on the driving temperature potential between the mainstream and coolant). The turbulence level at the entrance to the combustor section, which was a result of the upstream perforated plate, was 3%.

The exit dimensions of the primary channel for the combustor simulator were matched to the inlet dimensions of the pre-existing large-scale turbine vane cascade section [13,14]. This existing cascade represents one sector of an engine with the correctly scaled span-to-chord and pitch-to-chord ratios. The combustor simulator's inlet cross section and overall length were designed based on aeroengine data. The combustor's inlet cross-sectional area was such that the width was chosen to be slightly larger than one sector (to allow for sidewall flow removal) and the height was 1.8 vane spans. The height of the simulator was chosen such that the aeroengine's acceleration parameter (K) through the combustor was matched through the simulator. These acceleration parameters were calculated based on the inlet flow and the added mass flow through the liners and dilution holes matching the simulator to the engine.

Design of Liner Panels and Dilution Holes. Other than performing the measurements in an actual operating engine, it is not feasible to provide a measurement environment with all of a turbine engine's conditions being matched. In designing this combustor simulator, the parameters that were chosen to match an early design of a prototypical combustor included the following: i) the acceleration parameter (K, as defined in the Nomenclature) through the combustor; ii) the scaled combustor exit velocity to insure the correct inlet Reynolds number for the turbine section; iii) the coolant-to-mainstream momentum flux ratios of the liner cooling holes and the dilution holes; iv) the percentage coolant mass flux addition to the primary flow by the liner cooling holes, exit slot, and dilution holes; v) the film-cooling staggered hole pattern shown in Fig. 3; and vi) geometric scaling for the film-cooling hole diameter and the exit slot geometry (9X). Note that the parameters for the prototypical engine combustor were for actual running (hot) operating conditions. The air loading parameter (ALP defined in the Nomenclature, Lefebvre [15]) for the engine simulated was 0.66×10^{-4} and for the wind tunnel design was 0.4×10^{-4}. The loading parameter η_θ (see Nomenclature) given by Walsh and Fletcher [16] for both the engine and wind tunnel simulation was 1.8.

The liners for the combustor simulator were a streamwise series of four different panels that started 2.7 vane chords (1.6 m) upstream of the turbine test section. The first two panel lengths were 41 cm while the third and fourth panels were 38 cm and 46 cm. The panels extended the full width of the test section. The first two panels were horizontal to maintain a constant cross-sectional area while the following two panels were inclined at 17 deg to match the correct flow acceleration. The panels were constructed of 1.27 cm thick urethane foam with a low thermal conductivity ($k=0.037$ W/mK) to allow for adiabatic surface temperature measurements. The dense matrix of film-cooling and dilution holes for each of the panels were cut into the urethane foam using a water jet.

Table 1 Operating conditions and geometry

	Engine			No Dilution			With Dilution		
	$\%\dot{m}_{ex}$	M	I	$\%\dot{m}_{ex}$	M	I	$\%\dot{m}_{ex}$	M	I
Panel 1	3	6.6	13	4	3.1	9.3	3	3.7	14
Panel 2	7	4.6	7	9	2.8	7.8	7	2.8	8
Panel 3	7	2.4	3	9	2.6	6.9	7	2	4
Panel 4	3	1.9	1.5	4	1.8	3.3	3	1.2	1.5
Dilution Row 1	17.5	18	100	—	—	—	17.5	10	100
Dilution Row 2	17.5	7	20	—	—	—	17.5	4.5	20
Exit Slot	1.4	—	—	2.1	—	—	1.4	—	—

The aforementioned parameters, listed in Table 1, are believed to provide a flow field representative to that entering into the turbine. Since the Mach number is generally quite low ($Ma<0.1$) in the combustor, this parameter is not relevant. Another parameter not being matched is the coolant-to-mainstream density ratios, which are typically quite high (between two and three). Although the density ratios are not matched, the jet-to-mainstream momentum flux ratios and percentage of mass flow addition by both the film-cooling and dilution holes are being matched. The momentum flux ratio is the parameter that most affects mixing characteristics of jets in cross-flow. The film cooling hole patterns, shown in Fig. 3, were configured in equilateral triangles and spaced evenly across the panel surface. The diameter of the cooling holes was 0.76 cm giving an $L/D=3.3$.

The dilution hole diameters were also designed to insure the percent mass addition of the dilution fluid and coolant-to-mainstream momentum flux ratios were matched to that of the engine. This first row of dilution holes has three holes evenly spaced with the center hole being aligned with the center of the simulator (and also, when present, the vane stagnation) and located at 42% of the combustor length (0.68 m) downstream of the start of the panels. The dilution holes in the first row have a diameter that is 8.5 cm. The second row of dilution holes was located on the third panel at 56% of combustor length (0.9 m) downstream of the start of the panels. The second row of dilution holes contained two holes having a diameter 12.1 cm. The two dilution holes were staggered with the first row of holes (and also, when present, at the midpitch of the two passages in the vane cascade). As illustrated in Fig. 2(a), the supply chamber for the dilution flow was required to be some distance from the hole exits giving an L/D ratio of 1.5 for both rows. For both rows of dilution holes, the top and bottom dilution holes were aligned with one another in the span and streamwise directions. Many combustors are designed with a swirler followed by dilution holes producing an opposite sense of rotation as the swirl thereby reducing the overall exiting swirl. Since a swirler was not included in this study, the dilution holes were aligned with one another with the aim of having only a small exit swirl.

In addition to liner cooling holes and dilution holes, secondary coolant flow was added to the primary passage through a slot at the exit of the combustor section, which is shown in Fig. 4. The purpose of the feed holes is to control the coolant mass flow from the slot and to provide impingement cooling on the backside of the liner. The pin fins provide a conduction path from the liner to reduce the liner metal temperature. The percent mass flow

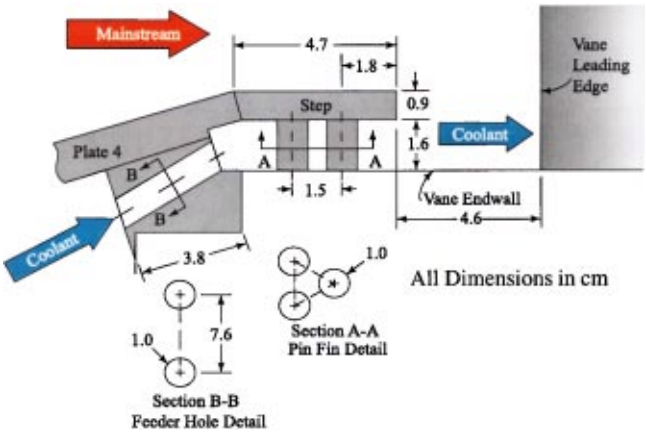

Fig. 4 Schematic illustrating the combustor liner exit slot

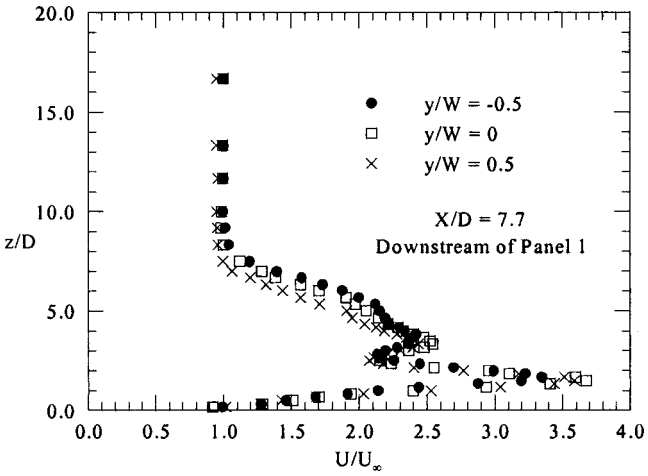

Fig. 6 Measured velocity profiles downstream of the first panel at three different spanwise positions

addition relative to the exit mass flow from this slot as well as all the panels was matched to that of the engine and is reported in Table 1.

Flow Control for the Liner Cooling, Dilution Holes, and Exit Slot. As indicated in Table 1, 44% of the flow from the fan is directed through the primary passage of the combustor simulator while 56% of the flow is directed through the secondary coolant passages to provide the flow for the liner coolant, dilution holes, and exit slot. The correct flows for each of the panels is set using previously determined discharge coefficients, the total pressure in each of the liner supply chambers ($P_{o,c}$), and the exit static pressure (p_∞). A number of experiments were conducted to evaluate the discharge coefficients for the liner cooling panels since it was suspected that an array of cooling holes would not necessarily have the same discharge coefficient as a single hole nor as a single row of holes. Measurements for the discharge coefficients were made using a laminar flow element (the true flow rate) the total pressure in the plenum, and the static pressure at the start of the film-cooling test plate.

To verify our capability in measuring discharge coefficients, comparisons were made to results presented in the literature by Burd and Simon [17]. Figure 5 shows these comparisons as well as the effect of the number of rows of film-cooling holes. Increasing the number of rows tends to slightly increase the discharge coefficient. This may be expected given the fact that as the number of rows of holes increases, the film layer increases causing a reduction in the resistance to the flow resulting in higher discharge coefficients.

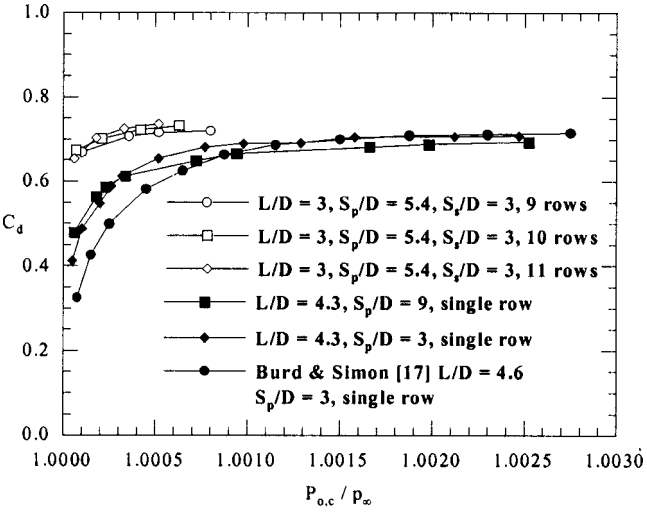

Fig. 5 Measured discharge coefficients of the film-cooling hole arrays

As mentioned earlier and indicated in Fig. 2(*a*), the flow to each of the liner panels comes from individually shutter-controlled supply chambers. Uniformity of the flow exiting the film-cooling holes for each panel was checked by taking a velocity profile with a hot-wire at the end of each panel liner. Figure 6 shows a representative sample of velocity profiles taken at three different spanwise locations downstream of the last row of film-cooling holes on the first panel. The data indicates uniformity among the holes and a double peak in the velocity profile resulting from the jet fluid from the upstream rows being pushed above the jet fluid exiting the last row of cooling holes.

The mass flow through the dilution holes were set by taking a velocity profile across the exit of the holes. There was a relatively large amount of flow exiting the dilution holes (35% of the total combustor exit flow) making it difficult to have a supply chamber large enough. The velocity profiles exiting the dilution holes were relatively flat, which allowed the flow rate for each dilution hole to be accurately calculated. The coolant flow rate through the slot was set by measuring the pressure drop across the feed holes shown in Fig. 4. Given that the feed holes were spaced significantly far apart (eight hole diameters), these feed holes were assumed to act as single holes having a discharge coefficient of 0.7.

Test Section Description. As discussed throughout this paper, the overall objective of these studies is to evaluate realistic combustor exit conditions on the development of the thermal and flow fields in a downstream turbine vane passage. Prior to making this evaluation for a turbine vane in which the flow experiences a large turning, a reference condition was chosen to be the combustor simulator followed by a straight test section with no vane present. By making adiabatic effectiveness measurements downstream of the combustor along a straight endwall with no turning, it provides a baseline for us to evaluate the maximum combustor liner coolant available for cooling the downstream platform. Because of the secondary flow patterns that develop in a vane passage, it is expected that this baseline would be somewhat higher than that which occurs in a vane passage.

The data presented in this paper is for the reference condition of a straight test section with no vane, as illustrated in Fig. 2(*e*). Note that for these measurements, the wind tunnel was converted to an open loop tunnel. This tunnel configuration had the advantage of allowing a long downstream test plate, but had the disadvantage of not allowing the use of a laser Doppler velocimeter due to the

seeding issue. The width and height of the downstream test section were 1.1 m and 0.55 m, respectively. The side and top walls were constructed from 1.27-cm thick acrylic. The bottom wall, which was the test plate, was a composite of 1.27-cm thick urethane foam ($k=0.037$ W/mK) on top with a 3.8-cm thick polystyrene plate as the next layer and a 1.9-cm plywood plate as the base. The top wall had a number of ports in which a crystal fluoride window could be placed for the infrared camera measurements.

Instrumentation and Uncertainty Estimates. Flow field data presented in this paper include measurements of the total pressure field and mean and turbulent velocities. Total pressure measurements were taken with a small Kiel probe having a head diameter of 1.6 mm. A small probe diameter was needed to insure good measurement resolution for the exit slot, which had a height of 16 mm. Streamwise mean velocity measurements were taken with a single hot-wire probe and a Pitot-static probe. Streamwise turbulence levels and length scales were measured using the single hot-wire probe. All of the pressure transducer and hot-wire voltages were converted to pressures and velocities using Labview software.

The mean thermal field and adiabatic surface temperatures were also measured. The thermal field data was collected using a rake having five type E thermocouples. The wire used to construct these thermocouples was 0.25 mm in diameter. To insure minimal conduction effects on the measured temperatures, the lead wires to the bead were bare thermocouple wires that were 6.35 mm long. The urethane foam test plate downstream of the combustor simulator was instrumented with type E thermocouples mounted flush with the surface. These measurements were compared with the surface temperatures measured using an infrared camera. When using the infrared camera, positioning crosses were placed on the endwall plate to scale and translate the pictures spatially. For each image, five pictures (with each picture being averaged over 16 frames) were needed to insure a good average for the surface temperatures. In some areas the pictures were overlapped resulting in a larger number of averages.

To set the flows in each of the supply chambers for the liners, pressure differences between the total pressure in the chamber and a static pressure at the start of the liner plate were measured. To insure the pressure taps were truly sensing the total and static pressures correctly, independent total and static pressures were compared to those made using a pitot-static probe. The differential pressure measurements for each of the supply chambers were read from calibrated transducers with a maximum range of 12.7 mm H_2O. As mentioned previously, the dilution flowrates were set by measuring the velocities at the exit of the dilution holes with a pitot-static probe. The pressure difference across the slot was measured using a transducer having a range of 127 mm H_2O.

The partial derivative and sequential perturbation methods, described by Moffat [18], were used to estimate the uncertainties of the measured values. Precision uncertainties were calculated based on a 95% confidence interval. For the streamwise velocities measured using the hot-wire, 100,000 samples were taken giving an uncertainty, including the bias and precision, of 1.8% for the mean velocity at a turbulence level of 14%. The precision uncertainty for the streamwise rms velocities was 2.6% at that same turbulence level. The integral length scales were calculated using eight samples of 80,000 data points taken at a sampling rate of 20,000 kHz giving a precision uncertainty of 15%. Each total pressure measurement used 60,000 data points to compute the mean values. The estimate of bias and precision uncertainties for the mean pressures, which were presented in non-dimensional form was 7.6% for a $\Delta P=-0.51$, which occurred in the near-wall region of interest. At lower ΔP values, the uncertainties were much higher such that for a $\Delta P=-0.14$, the uncertainty is 27%. The bias and precision uncertainties on the adiabatic effectiveness values, using the five-averaged pictures, was ± 0.038 giving an uncertainty of 6.5% at $\eta=0.59$. The thermal field contour uncertainties, including both bias and precision, at a level of $\theta=0.52$ was 8.2%.

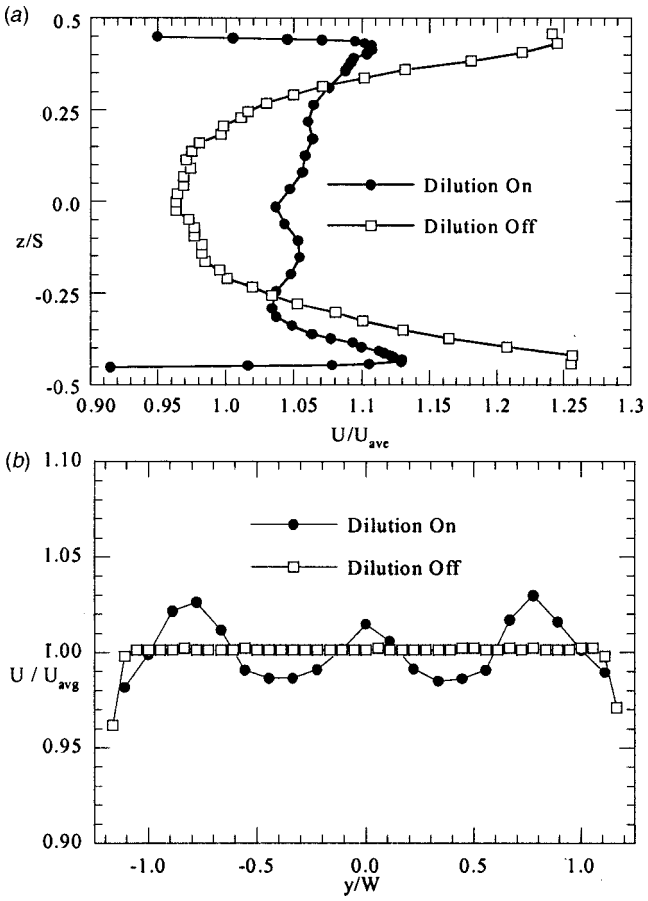

Fig. 7 Mean velocity profiles measured at the exit of the simulator in the span (*a*) and pitch (*b*) with, and without the dilution jets

Experimental Results

As previously mentioned, the data that will be presented in this paper is for the case with no turbine vane present downstream of the combustor simulator. The focus of the results in this paper is on the effects of the dilution jets with regards to the exiting downstream flow and thermal fields. The flow conditions for the two cases are given in Table 1. Note that the two flow conditions, i.e., dilution and no dilution, were achieved by maintaining nearly the same combustor exit velocity thereby requiring a higher inlet velocity for the combustor simulator in the no dilution case. Total pressure, mean and turbulent velocities, and the thermal field were measured in a plane normal to the flow direction either on top of the step or downstream of the slot with both locations being illustrated in Fig. 2(*b*). The downstream location corresponds to the stagnation location of the first vane (if it were present). The measurement plane on top of the step was located five cooling hole diameters upstream of the slot exit ($x/D=-5$, where x is measured from the slot exit), which is 14 cooling hole diameters downstream of the last row of cooling holes on the last panel. Adiabatic effectiveness measurements were made on the plate downstream of the slot.

Flow Field Results. For the conditions without the vane being present, the flow is expected to be symmetric about the midspan and about the midpitch of the test section. The midspan symmetry was verified experimentally and is shown in Fig. 7(*a*)

for the dilution and no dilution cases, while the midpitch symmetry is shown in Fig. 7(*b*). These profiles were taken at a streamwise distance of $x/D=-5$. The spanwise velocity profile (Fig. 7(*a*)) was taken at the midpitch location of the test section, which is aligned with the center of the dilution hole in the first row of dilution holes (and when present the stagnation location of the turbine vane). The pitchwise velocity profile was taken at the midspan of the test section. Note that $z/S=0.5$ corresponds to the endwall location and since this data was taken on top of the slot, the values measured at the wall correspond to a location that is slightly above zero at $z/S=0.455$.

Figure 7 shows very different velocity characteristics for the dilution on and off cases at this location. For the spanwise (radial) profile (Fig. 7(*a*)), the effect of the dilution jets was to flatten out the profile across the span relative to the no dilution case. It is clear that in both cases, there is still a higher speed fluid in the near wall resulting from the coolant injection. The pitchwise (circumferential) profiles (Fig. 7(*b*)), indicate a variation in the velocities for the dilution hole case. The lower velocities in Fig. 7(*b*) correspond to the locations of the second row of dilution holes. Although the second row of dilution jets has a lower momentum flux ratio than the first row of jets, the second row is directed somewhat upstream because of the angle of the third panel. This represents a flow blockage in the mainstream resulting in lower velocities.

Turbulence profiles, based on the measured streamwise rms levels and local mean velocities, are given in Figs. 8(*a*) and (*b*) for the same locations as given in Fig. 7. Since the geometry being used in this study is representative of a combustor, the exiting turbulence levels should be indicative of those found entering the turbine of an engine. Evidence in the literature suggests that the same turbulence levels exist whether combustion is present or not (Zimmerman [19] and Moss [20]). The effect of the dilution jets at this location is to elevate the turbulence level range to be between 15–18%. For the spanwise turbulence profile (Fig. 8(*a*)), the turbulence from the upstream film cooling holes in the near wall region affects the span as high as 25% for the no dilution case with the turbulence levels being higher in the near wall region. The effect of the dilution jets is such that the turbulence in the mainstream is higher than in the near wall region and with the decrease starting at 20% of the span. The pitchwise profiles in Fig. 8(*b*) show two peaks that correspond to the two dilution hole locations in the second row.

Also shown in Fig. 8(*b*) are the measured integral length scales across the pitch at the mid-span of the test rig. These integral length scales were normalized using the diameter of the dilution hole in the first row. As seen on Fig. 8(*b*), the length scale is on the order of the diameter of the dilution hole. It has long been a question among the turbine community as to what is the correct turbulent length scale to simulate. These results, along with the results previously reported by Moss [20], indicate that the integral length scale is a strong function of the dilution hole size. Also shown in Fig. 8(*b*) is an increase in the integral length scale at $y/W=0.25$, which corresponds to the second row of dilution holes. Note that the dilution hole diameter for the second row is 42% larger while the length scale in this region increased by 20%. These length scales can be compared to those simulated in the previous work by Radomsky and Thole [13,14]. While the length scales for the previous work were 10% of the turbine vane pitch, the length scales measured in the current study would be somewhat larger at 14% of the turbine vane pitch.

Figure 8(*c*) shows the energy spectra of the turbulence at the combustor exit for a location with the largest length scale and smallest length scale. While the spectra shows a typical $-5/3$ region and does agree with the von Karman spectra, the inertial subrange extends less than two decades. This is in contrast to the data previously reported by Radomsky and Thole [13] for a turbulence level of 19.5% achieved using their active turbulence generator grid. Results using the active grid showed an inertial subrange that extended slightly more than two decades. These results indicate that at this location the viscous dissipation occurs at lower wave numbers as compared with the active grid results.

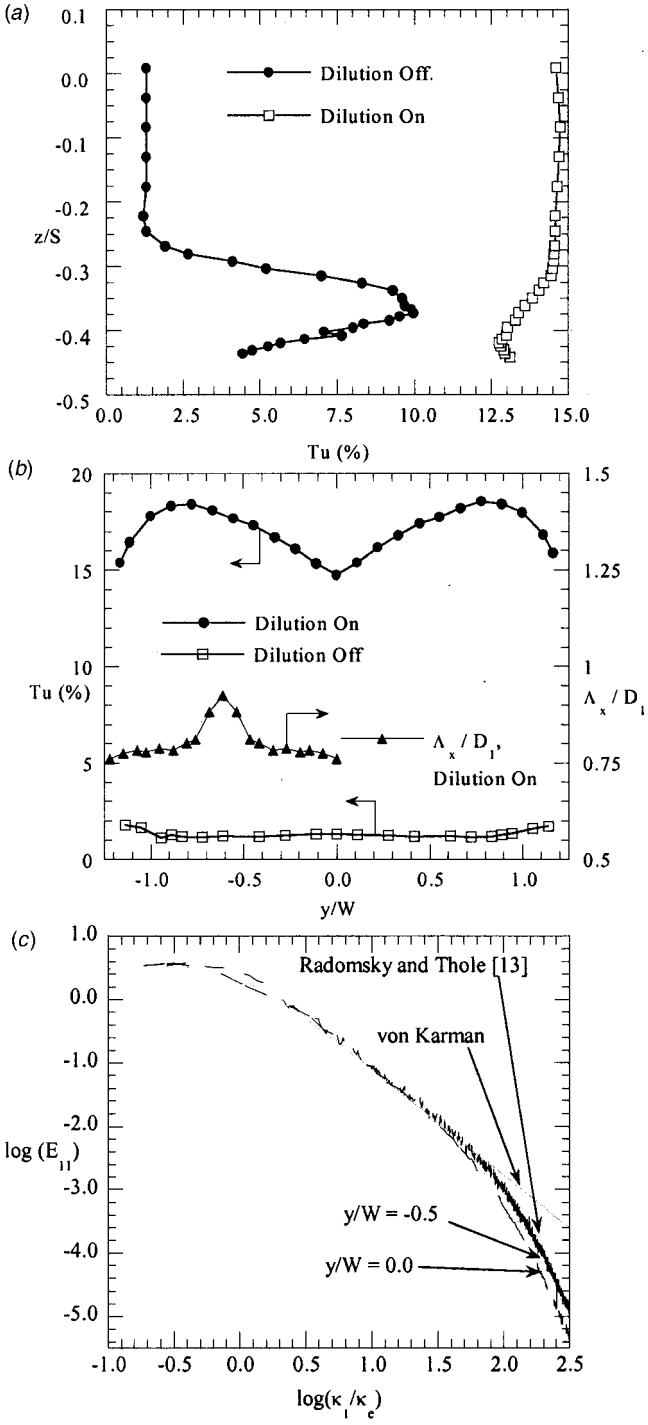

Fig. 8 Turbulence profiles measured at the exit of the combustor simulator in the span (*a*) and pitch (*b*), and streamwise velocity energy spectra (*c*)

Figure 9 shows contours of the normalized streamwise velocity and the local turbulence level for the dilution case. The measured contours given in Fig. 9 were in a plane that was one-quarter of a turbine sector in the pitch (y/W) direction and one-half of a turbine vane span in the Z/S direction. Note that this portion of the exit plane can be mirrored due to symmetry conditions. These measurements were made at a streamwise position relative to the

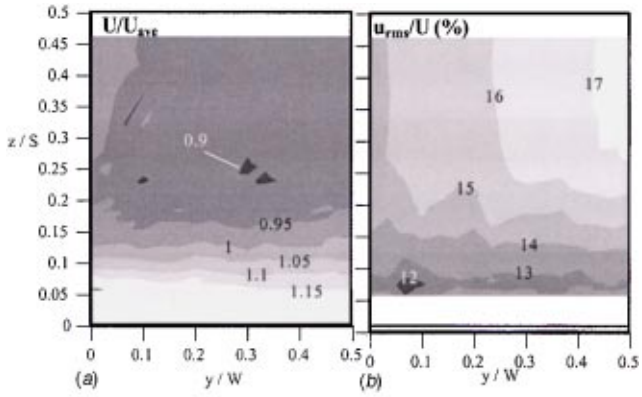

Fig. 9 Contours of normalized streamwise velocity (*a*) and turbulence levels upstream of the slot exit (*b*) for the dilution flow case

end of the slot at $x/D=-5$. Figure 9(*a*) still shows slight remnants of the dilution jets, but with a larger variation in the near wall region as a result of the film cooling injection. The turbulence level contours show a variation from the 14.5–18% with the peak aligned with the center of the dilution jet in the second row. Since the highest turbulence level is associated with the dilution hole, the highest turbulence level would be expected to be at the vane stagnation if the vane were clocked with a dilution hole. This is important to recognize in terms of the high heat transfer augmentation that would occur at the vane leading edge. In general, the lowest turbulence levels are in the near wall region.

As can be seen in Fig. 9 there is a large variation of the velocity and turbulence across the pitch (y/W). For this region, total pressures at the slot exit were measured at a position near the top of the slot. These total pressure variations are presented in Fig. 10 along with a schematic illustrating the feed holes and pin fin locations. The variation in total pressure is quite large and is somewhat periodic corresponding to the feed hole locations. CFD results (which are not presented in this paper) have indicated that the flow exiting the slot is dependent on how the feed holes are aligned with the pin fins and how the secondary flows from the dilution jets interact with the exit slot flow.

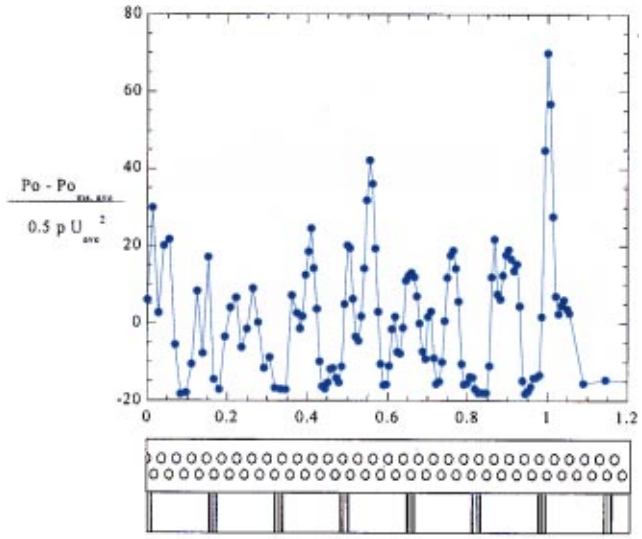

Fig. 10 The nonuniform total pressure profile across the pin-finned exit slot. Below the plot is an indication of where the pin fins and slot feeder holes are located.

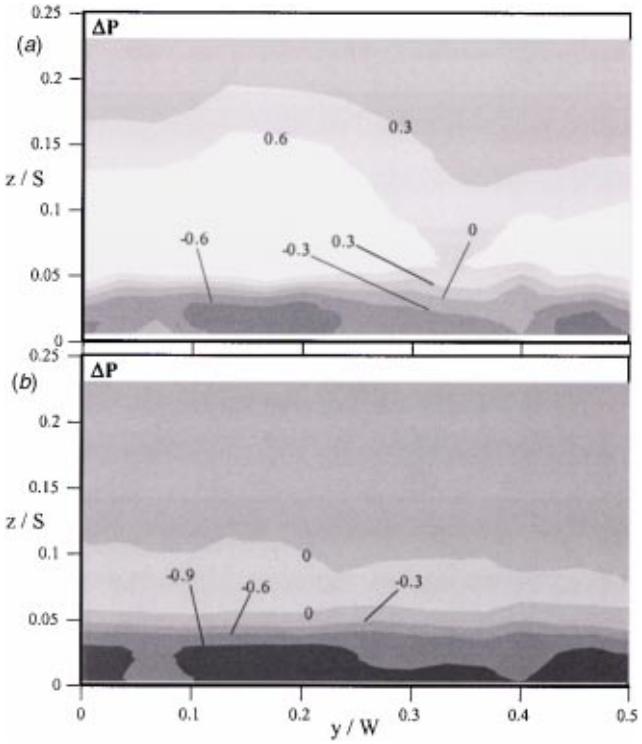

Fig. 11 Nondimensional total pressure profiles of the exit slot for the no dilution (*a*) and dilution cases (*b*)

Contours of the normalized total pressure for the no dilution and dilution cases are shown in Fig. 11. The location for these measurements corresponds to 2.9 step heights downstream of the slot. The differences between the no dilution and dilution cases are quite drastic. While in both cases the total pressure in the near wall region is the lowest pressure, the pressure variation above the slot location is much larger for the no dilution case than for the dilution case. These differences are caused by the effects of the dilution mixing and by the fact that there is a slightly higher momentum flux ratio for the jets exiting the last panel for the no dilution case. There is only a slightly higher total pressure region above the slot for the dilution flow case. The dilution flow enters the combustor with a relatively high total pressure, which in turn raises the total pressure in the primary flow path. As a result, the total pressure variation in the span direction (z/S) is reduced.

Figure 12 presents a pitchwise-averaged, nondimensional total pressure for the dilution and no dilution cases as compared with a total pressure profile if assuming a two-dimensional, turbulent boundary layer. The turbulent boundary layer profile is for a boundary layer having a thickness that is 9% of the span having an $\mathrm{Re}_\theta=3400$. Figure 12 indicates a larger variation for the no dilution case as compared with the dilution case. Neither of these profiles, however, are similar to what occurs for a turbulent boundary layer approaching the vane. Figure 12 indicates that there is an increase in the total pressure followed by a decrease as the wall is approached. It is expected that the resulting secondary flow pattern developing in the turbine would not be the same as that with a turbulent boundary layer.

Thermal Field Results. As mentioned previously in this paper, a heater in the primary flow path and heat exchangers in the secondary flow paths allow for thermal field simulations. For these experiments, the primary flow was heated to levels that were nominally 16°C above the coolant temperatures. The measured thermal fields for the no dilution and dilution cases are given in Fig. 13 for the downstream slot location. Note that the freestream temperature used in the thermal field normalization (θ) and for the

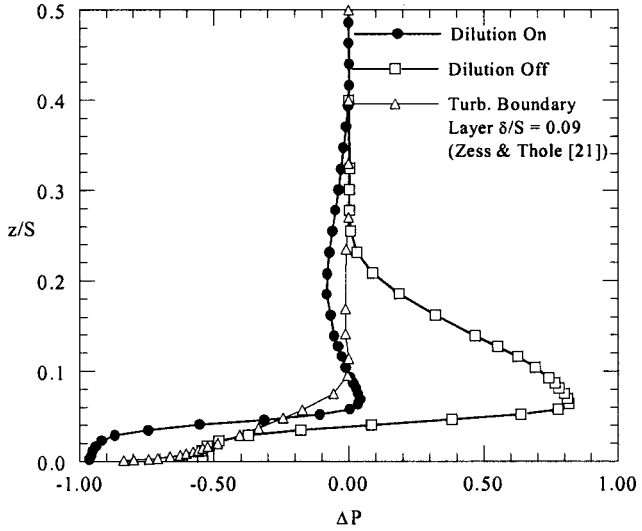

Fig. 12 Spatially averaged nondimensional total pressure profiles downstream of the combustor liner slot for the no dilution and dilution cases compared to a turbulent boundary layer [21]

adiabatic effectiveness levels (η) was based on the mass averaged temperature for the dilution flow case. Since much of the flow at the combustor exit is from either the cooling liner or from the dilution holes, the overall freestream temperature was reduced. To account for this reduced temperature, the mass averaged temperature was calculated and used with the coolant temperature as the driving temperature potential. For the no dilution flow, the freestream temperature used is the temperature of the flow just downstream of the heaters. For the case with no dilution, Fig. 13(*a*) shows that there is very good coverage of the downstream endwall plate. The spanwise extent of the $\theta = 0.7$ level was as high

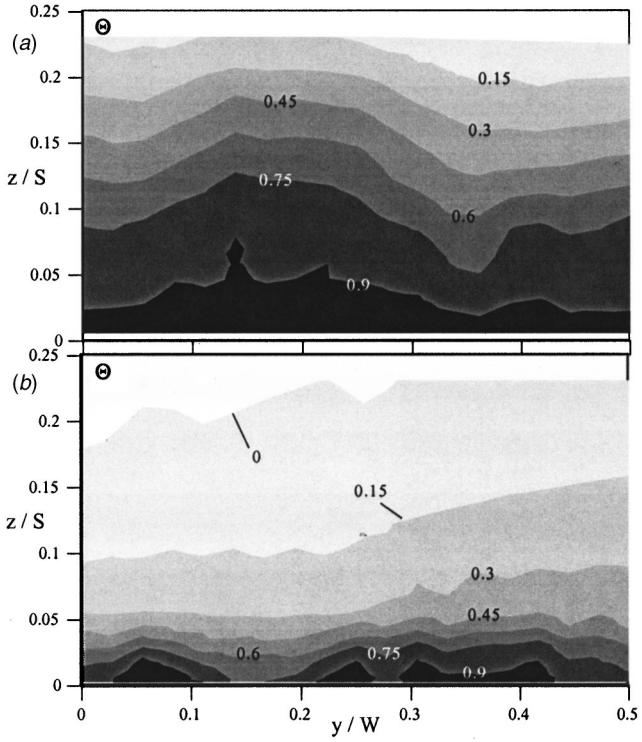

Fig. 13 Nondimensional thermal field contours after the exit slot for no dilution (*a*) and dilution (*b*)

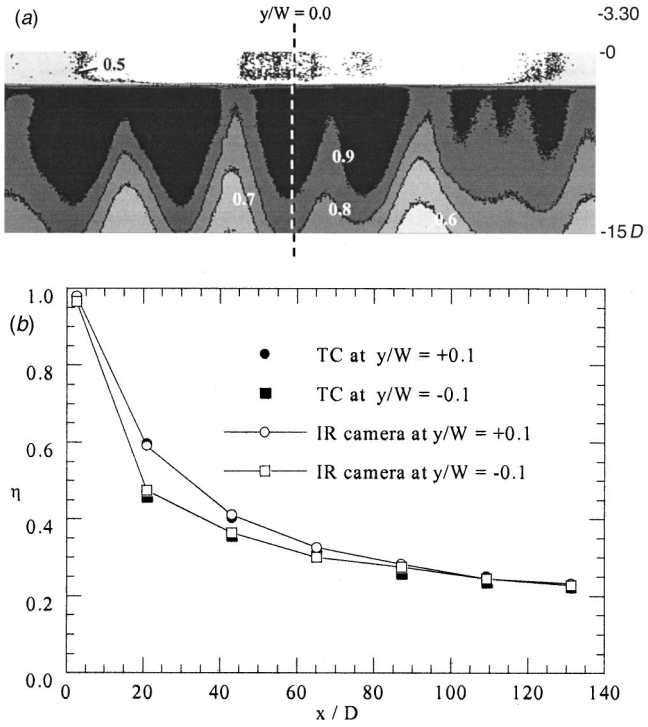

Fig. 14 Adiabatic effectiveness contours (*a*) and downstream levels (*b*) on the endwall for the case with dilution jets

as $z/S = 0.1$ for the no dilution case. In comparison, the case with dilution indicates much less coolant along the endwall as shown in Fig. 13(*b*). The thermal field for the dilution case also shows the slightly cooler temperatures apparent in the main flow as a result of the second row dilution jets.

Adiabatic effectiveness contours close to the slot exit are given in Fig. 14(*a*)(*b*) for the dilution flow case. Note that the first 3.3*D* streamwise distance are contour levels that were measured on top of the pin fin liner plate. The high adiabatic effectiveness levels (~0.5) are from the remnants of the upstream film-cooling holes on the pane. Downstream of the slot, it is quite apparent as to the non-uniformity of the slot exit flow based on the local adiabatic effectiveness levels. The levels just downstream of the slot are quite high even at the location where the leading edge of the vane would be placed ($x = L$).

Figure 14(*a*)(*b*) shows the downstream adiabatic effectiveness levels measured using an IR camera as compared with thermocouples (TC) that are embedded in the surface of the urethane foam endwall plate. There is good agreement between the IR camera and thermocouple measurements at the two different pitchwise positions. Note that both of these pitchwise positions are slightly off the centerline of the endwall test plate and do indicate some variation in the pitch. This is to be expected based on Fig. 14(*a*). At 100*D* downstream, the two different pitchwise measurements indicate the same level suggesting a more uniform coverage. To give a perspective on these distances, a streamwise distance of 130*D* (the last measurement location) corresponds to 1.8 true chord lengths downstream of the turbine vane. At 130*D* downstream, the adiabatic effectiveness levels are still 0.2 indicating that there is a potential for using the combustor liner fluid to cool the downstream turbine platform if there were no secondary flows present in the vane passage.

Conclusions

This paper describes the development of a scaled-up test rig that simulates the aft end of a gas turbine engine combustor. Flow and thermal field measurements were made at the exit of the simu-

lator to determine prototypical conditions for the downstream turbine. These tests were conducted with no turbine vane present to provide a baseline for comparison. With no downstream turbine vane present, the measured adiabatic effectiveness levels on the downstream endwall represent the best that could be achieved along the vane passage endwall if no secondary flows are present.

The results of these measurements put in question the accuracy in assuming either a constant total pressure field or a turbulent boundary layer approaching the turbine vane-endwall juncture. The total pressure field measurements clearly showed a profile much different than would be present for either of the two previously stated assumptions. While the effect of the dilution jets was to reduce the variations in the total pressure and velocity field, there was still some variation in the near-wall region. The measured turbulence indicates that levels entering the turbine for this type of configuration are between 15–18%. The results in this paper also indicate that the length scale of the turbulence scales closely with the turbulence producing mechanism, namely the dilution hole diameter. This latter result is important because generally the dilution hole diameter is known for a particular turbine engine design thus providing information for more accurate heat transfer predictions.

The thermal field contours indicated that the dilution jets increased the mixing of the coolant exiting the slot and the upstream film cooling holes, thereby reducing the coolant available for cooling the downstream platform. Although there was a reduction, the adiabatic effectiveness levels along the downstream platform were still quite high at what would be one chord downstream of the slot exit if the vane were present.

Acknowledgments

The authors gratefully acknowledge United Technologies—Pratt & Whitney for their support of this work. Guidance was received throughout this project from A. Cheung, A. Kohli, M. Ondus, F. Soechting, J. Wagner, and G. Zess.

Nomenclature

ALP = air loading parameter, $\mathrm{ALP}=P_o^{1.75}A_{\mathrm{ref}}D_{\mathrm{ref}}^{0.75}e^{T/300}/\dot{m}$
C = true chord of stator vane
C_d = discharge coefficient, $C_d=\dot{m}/A_{\mathrm{hole}}\sqrt{2\rho(P_{o,c}-p_\infty)}$
D = film cooling hole diameter
D_1, D_2 = dilution hole diameters for first and second rows
$E(\kappa)$ = energy spectra of streamwise fluctuations
E_{11} = defined as $E_{11}=2\pi E(\kappa)/u_{\mathrm{rms}}^2\Lambda_x$
f = frequency
H = test section height
I = momentum flux ratio, $I=\rho_c U_c^2/\rho_\infty U_\infty^2$
K = acceleration parameter defined as $K=(\nu dU_\infty/dx)/U_\infty^2$
k = thermal conductivity
L = film cooling hole length
$\dot{m}$ = mass flow rate
M = mass flux ratio, $M=\rho_c U_c/\rho_\infty U_\infty$
P = vane pitch
P_o, p = total and static pressures
R = gas constant
Re = Reynolds no. defined as $\mathrm{Re}=CU_\infty/\nu$
s = surface distance along vane measured from flow stagnation
S = span of stator vane
S_s, S_p = streamwise, pitchwise film cooling hole spacing
T = temperature
T_{inf} = mass averaged freestream temperature
Tu = turbulence level defined as u_{rms}/U
u_{rms} = root mean square of velocity fluctuations
U = local, mean streamwise velocity component
W = turbine sector width
X,Y,Z = global coordinates defined in Fig. 2(*a*)
x,y,z = local coordinates
η = adiabatic effectiveness, $\eta=(T_{\mathrm{inf}}-T_{\mathrm{aw}})/(T_{\mathrm{inf}}-T_c)$
η_θ = loading parameter, $\dot{m}/(\mathrm{Vol}\ P_o^{1.8}10^{0.00145(T-400)})$
κ = wave number, $\kappa=2\pi f/U$
ΔP = nondimensional pressure, $\Delta P=(P_o-\overline{P_{o,\mathrm{ms}}})/(0.5\rho U_{\mathrm{ave}}^2)$
Λ_x = integral length scale
ρ = density
ν = kinematic viscosity
θ = nondimensional temperature, $\theta=(T_{\mathrm{inf}}-T)/(T_{\mathrm{inf}}-T_c)$

Subscripts

1,2 = dilution row 1 and 2
ave = spatial average
aw = adiabatic wall
in = inlet location of combustor simulator
ms = midspan
ref = combustor reference dimensions
rms = root mean square
ex = exit location of combustor simulator
inf, ∞ = freestream conditions
c = coolant conditions

References

[1] Langston, L. S., 1980, "Crossflows in a Turbine Cascade Passage," ASME J. Eng. Power, **102**, p. 866.
[2] Kang, M., and Thole, K. A., 2000, "Flowfield Measurements in the Endwall Region of a Stator Vane," ASME J. Turbomach., **122**, pp. 458–466.
[3] Munk, M., and Prim, R. C., 1947, "On the Multiplicity of Steady Gas Flows Having the Same Streamline Pattern," Proc. National Academy of Sciences, **33**.
[4] Shang, T., and Epstein, A. H., 1997, "Analysis of Hot Streak Effects on Turbine Rotor Heat Load," ASME J. Turbomach., **119**, pp. 544–553.
[5] Hermanson, K., and Thole, K. A., 2000, "Effect of Inlet Profiles on Endwall Secondary Flows," J. Propul. Power, **16**, pp. 286–296.
[6] Butler, T. L., Sharma, O. P., Joslyn, H. D., and Dring, R. P., 1989, "Redistribution of an Inlet Temperature Distortion in an Axial Flow Turbine Stage," J. Propul. Power, **5**, pp. 64–71.
[7] Shang, T., Guenette, G. R., Epstein, A. H., and Saxer, A. P., 1995, "The Influence of Inlet Temperature Distortion on Rotor Heat Transfer in a Transonic Turbine," AIAA Paper No. 95- 36318.
[8] Stabe, R. G., Whitney, W. J., and Moffitt, T. P., 1984, "Performance of a High-Work Low Aspect Ratio Turbine Tested with a Realistic Inlet Radial Temperature Profile," NASA Technical Memorandum 83655, AIAA Paper No. 84-1161.
[9] Burd, S., and Simon, T., 2000, "Effects of Slot Bleed Injection Over a Contoured Endwall on Nozzle Guide Vane Cooling Performance: Part I—Flow Field Measurements," ASME Paper No. 2000-GT-199.
[10] Burd, S., Satterness, C., and Simon, T., 2000 "Effects of Slot Bleed Injection Over a Contoured Endwall on Nozzle Guide Vane Cooling Performance: Part II—Thermal Measurements," ASME Paper No. 2000-GT-200.
[11] Soechting, F. O., and Cheung, A., 1999, private communication at Pratt & Whitney.
[12] Kang, M., Kohli, A., and Thole, K. A., 1999, "Heat Transfer and Flowfield Measurements in the Leading Edge Region of a Stator Vane Endwall," ASME J. Turbomach., **121**, pp. 558–568.
[13] Radomsky, R., and Thole, K. A., 2000, "Highly Turbulent Flowfield Measurements Around a Stator Vane," ASME J. Turbomach., **122**, pp. 255–262.
[14] Radomsky, R., and Thole, K. A., 2000, "High Freestream Turbulence Effects in the Endwall Leading Edge Region," ASME J. Turbomach. (2000-GT-202), **122**, pp. 699–708.
[15] Lefebvre, A. H., 1998, *Gas Turbine Combustors*, Taylor and Francis, New York, NY.
[16] Walsh, P. P., and Fletcher, Pl, 1998, *Gas Turbine Performance*, Blackwell Science LTD, NJ.
[17] Burd, S., and Simon, T., 1999, "Measurements of Discharge Coefficients in Film Cooling," ASME J. Turbomach., **121**, pp. 243–248.
[18] Moffat, R. J., 1988, "Describing the Uncertainties in Experimental Results," Electronics, **1**, pp. 3–17.
[19] Zimmerman, D. R., 1979, "Laser Anemometer Measurements at the Exit of a T63-C20 Combustor," National Aeronautics and Space Administration, NASA Lewis Research Center, Contract NAS 3-21267.
[20] Moss, R. W., 1992, "The Effects of Turbulence Length Scale on Heat Transfer," University of Oxford, Department of Engineering Science, Report No. OUEL 1924, Ph.D. dissertation.
[21] Zess, G. A., and Thole, K. A., 2002, "Computational Design and Experimental Evaluation of a Leading Edge Fillet on a Gas Turbine Vane," ASME J. Turbomach. (2001-GT-404), **124**, pp. 167–175.